Technical University of Denmark

**DTU**

# Characterisation of low temperature surface hardened stainless steel

**Christiansen, Thomas Lundin; Somers, Marcel A. J.**

*Published in:*
E-structure

*Publication date:*
2006

*Document Version*
Publisher's PDF, also known as Version of record

Link back to DTU Orbit
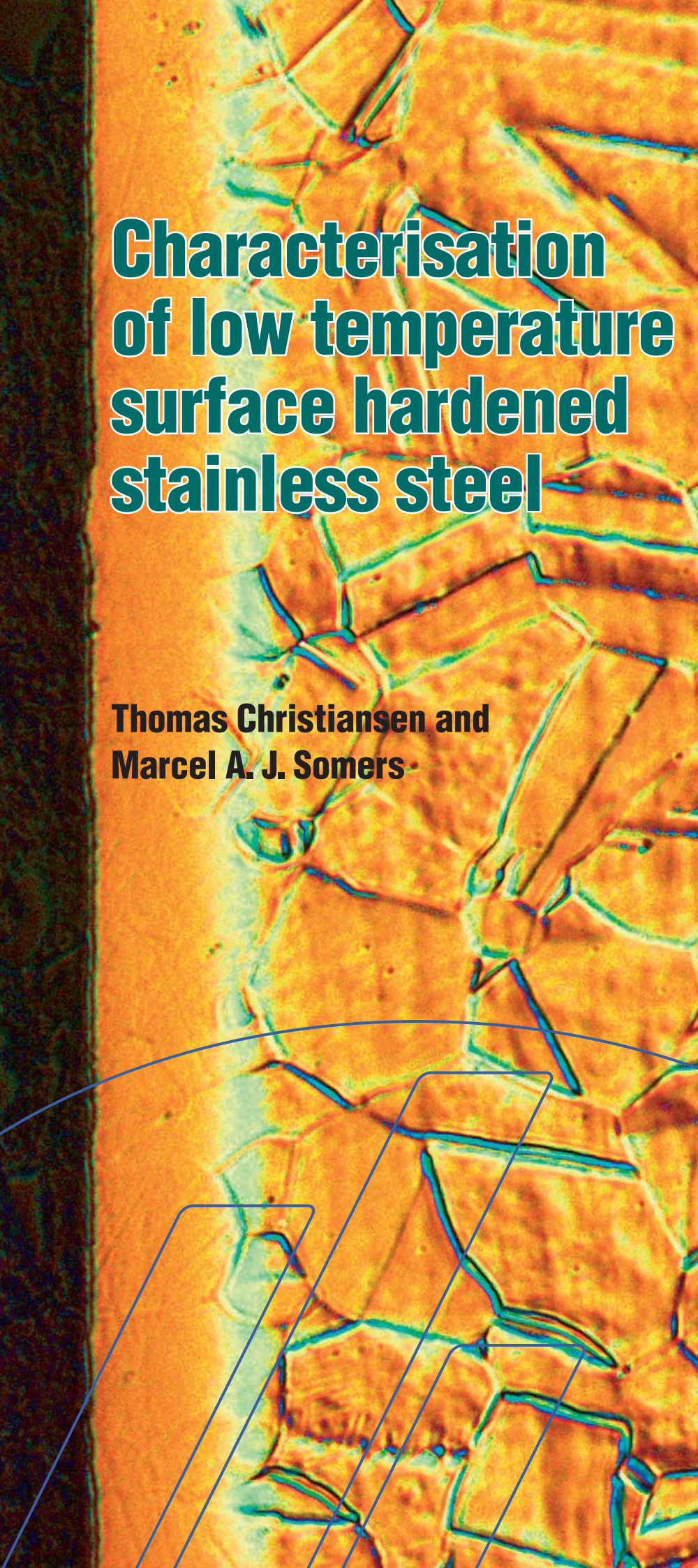
**DTU Library**
Technical Information Center of Denmark

# Characterisation of low temperature surface hardened stainless steel

**Thomas Christiansen and Marcel A. J. Somers**

# Characterisation of low temperature surface hardened stainless steel

*Thomas Christiansen, tc@ipl.dtu.dk*
*and Marcel A. J. Somers, somers@ipl.dtu.dk*

*Technical University of Denmark,*
*Department of Manufacturing Engineering and Management*
*Kemitorvet b. 204*
*DK-2800 Kgs. Lyngby*
*Denmark*

## 1. Introduction

Stainless steel is a widely applied material in applications where corrosion resistance is of importance. The corrosion resistant nature of stainless steels has its origin in the presence of the alloying element Cr, which forms a very stable passive layer that protects the steel. Unfortunately, stainless steel suffers from extensive wear e.g. galling, which hinders a wider applicability of the material and may cause problems in existing applications. Common practice for improvement of surface properties of steels, with respect to wear, comprises surface engineering. Traditional gaseous thermochemical treatments for surface engineering are typically carried out in carbon and/or nitrogen bearing gases and are usually associated with temperatures above 773 K, e.g. nitriding, carburising and nitrocarburising. The improvement of wear properties (and hardness) relies on the development of a compound layer and an underlying diffusion layer in the surface adjacent region of the sample. However, stainless steel poses two problems in this respect: Firstly, it is difficult to harden the surface by gaseous thermochemical treatment as the native passive layer is impenetrable for nitrogen and carbon atoms. Secondly, (traditional) gaseous thermochemical treatment is associated with a loss of corrosion resistance as nitrogen and carbon react with chromium to form carbides/nitrides, thus redrawing chromium from solid solution. As a consequence, surface hardening of stainless steel by thermochemical treatment has been considered bad practice or a compromise between corrosion properties and tribological properties, as surface engineering invariably impairs the corrosion resistance.

In the mid-eighties it was discovered that at temperatures below approximately 723 K it was possible to dissolve large quantities of nitrogen or carbon in the stainless steel by plasma nitriding or plasma carburising. The resulting surface structures of plasma-treated stainless steel proved exceptionally wear resistant and the corrosion resistance was unaltered or even improved. Plasma/implantation based techniques solve the problem of the passive layer impenetrability as the oxide layer is removed by sputtering as an integrated

part of the process. However, plasma/implantation based techniques suffer from, in particular, ill-defined thermodynamics and constraints on the sample geometry. Gaseous thermochemical processes are not subjected to such disadvantages.

The microstructural feature responsible for the highly demanded combination of excellent corrosion and wear performances is the expanded austenite, $\gamma_x$ (X=N,C) hitherto also called S-phase [1,2,3]. Expanded austenite without nitrides/carbides is obtained when high amounts of atomic nitrogen and/or carbon are dissolved in stainless steel at temperatures below, say 723 K for nitrogen and about 823 K for carbon. The nitrogen/carbon atoms are presumed to reside in the octahedral interstices of the f.c.c. lattice [3]. Long range order among the nitrogen/carbon atoms has so far not been confirmed with X-ray diffraction techniques. Typically, nitrogen contents in expanded austenite range from 20 to 30 at.% N; carbon contents range from 5 to 12 at.% C [4,5,6]. In terms of N:Cr ratio the homogeneity range of nitrogen-expanded austenite spans from approximately 1:1 to 3:1 [7].
Expanded austenite is metastable and tends to develop chromium-nitrides/carbides [8,9,10]. The high interstitial content of C/N is obtained, because of the relatively strong affinity of Cr atoms for N and (to a lesser extent) C atoms, leading to anticipated short range ordering of Cr and N/C. Due to the low mobility of Cr atoms as compared to interstitial N/C atoms at low treatment temperatures, chromium nitrides/carbides do not precipitate until after long exposure times and N/C is kept in solid solution by the Cr "trap sites".

Hardness values up to 1700 HV have been reported for nitrided austenitic stainless steel [11,12]; the strengthening mechanism has so far not been elucidated. Most likely solid-solution hardening by the high interstitial atom content is dominant; the occurrence of an enhanced stacking fault density in austenite may contribute to strengthening.
Spectacular wear reductions of several decades have been reported for stainless steels nitrided under conditions where expanded austenite develops [13,14]. In the worst case the electrochemical properties remain unaltered, but they can be improved, in particular the pitting potential [15,16].

Recently an ex-situ pre-treatment of stainless steel was developed, which enables subsequent low temperature gaseous nitriding and/or carburising and allows controlled formation of an expanded austenite layer [17]. The pre-treatment entails stripping the surface of the passive oxide layer and depositing a nanometre-scale thin catalytic

layer, e.g. Ni. The role of the catalytic layer is twofold: preventing the stainless steel surface from repassivation and catalyzing the dissociation of the gas species at the surface, thus promoting the surface kinetics and allowing processing at lower temperatures.

The present article elucidates the possibilities of this newly developed method for gaseous thermochemical processing.

## 2. Experimental

Experimental work was carried out with both millimetre-sized bulk samples and micrometer-sized thin film material. Thin films were applied for through-nitriding experiments, i.e. for synthesizing homogeneous expanded austenite.

The (nominal) compositions of the investigated stainless steel bulk samples are given in Table 1 and the compositions of the certified stainless steel thin foils are given in Table 2.

The bulk samples were sliced into discs, typically with a diameter of 13 mm and a thickness of 2-3 mm, and subsequently ground/polished with successively finer emery paper/diamond paste (see preparation for reflected light microscopy below). Not all samples were polished with diamond paste; SAF 2507 was neither ground nor polished. The stainless steel thin foil material was austenitised at 1343 K in pure $H_2$. During austenitisation the deformation-induced martensite, which was introduced upon cold-rolling during the manufacturing of the foils, was totally transformed to austenite.

Bulk and thin foils samples were pre-treated to allow gaseous thermochemical treatment in a carbon and/or nitrogen containing atmosphere [17].

| Alloy | Mn | Si | Cr | Ni | Mo | Other | Fe |
|---|---|---|---|---|---|---|---|
| AISI 304 | 2 | 1 | 18-20 | 8-10.5 | - | - | Balance |
| AISI 316 | 2 | 1 | 16-18 | 10-14 | 2-3 | - | Balance |
| AISI 329 | 1 | 0.75 | 23-28 | 2.5-5 | 1-2 | - | Balance |
| SAF 2507 | 1.2 | 0.8 | 25 | 7 | 4 | N: 0.3 | Balance |
| Uddeholm Corrax® | 0.3 | 0.3 | 12 | 9.2 | 1.4 | Al: 1.6 | Balance |
| Sandvik Nanoflex® | 0.5 | 0.5 | 12 | 9 | 4 | Cu: 2 Ti: 0.9 Al: 0.4 | Balance |

*Table 1: Nominal composition of the investigated bulk stainless steels in wt.%.*

| Alloy | Cr | Ni | Mo | Mn | Si | Fe |
|---|---|---|---|---|---|---|
| AISI 304L | 19.45 | 9.49 | 0 | 1.17 | 0.98 | Balance |
| AISI 316L | 18.93 | 13.55 | 1.69 | 1.76 | 0.62 | Balance |

*Table 2: Composition of stainless steels thin foils in atomic %. The compositions were certified by Sandvik Materials Technology*

Nitriding was performed in mixtures of $NH_3$ and $H_2$ (and a small flow of $N_2$ in the thermobalance), the partial pressures of $H_2$ and $NH_3$ determine the so-called nitriding potential, $K_N = p_{NH_3} / p_{H_2}^{3/2}$; the dimension of the nitriding potential is bar $^{-1/2}$. Carburising was performed in mixtures of CO and $H_2$, the partial pressures of CO and $H_2$ are contained in the so-called carburising potential, $K_C = p_{CO} \, p_{H_2} / p_{H_2O}$; the dimension of the carburising potential is bar. Since the partial pressure of $H_2O$ was not adjusted and therefore unknown the carburising potential is not known. For the special case of carburising in 100% CO the carburising potential corresponds to infinity, assuming that no soot is formed during carburising, which would reduce the carbon activity imposed onto the stainless steel surface to 1 (with reference to graphite). Nitrocarburising was carried out in an atmosphere of $NH_3$, $C_3H_6$, $H_2$ and Ar.

A Netzsch STA 449C thermal analyzer capable of performing differential and thermogravemetric analysis simultaneously was applied for thermochemical treatment and thermal analysis. Occasionally, a custom built furnace with 6 heating zones was applied for thermochemical treatment.

The thermochemically treated samples were cross-sectioned and hot mounted in a Struers Prontopress. Struers DuroFast black resin was used for hot mounting for optimal edge retention. The hot-mounting procedure consisted of preheating without pressure for 4 minutes (453 K) followed by heating with a pressure of 20 kN/mounting area for 6 minutes (453 K) and finally 5 minutes of cooling. Grinding and polishing were carried out on a Struers Abramin. The procedure for metallographic preparation is given in Table 3. The applied etching agent used for revealing the microstructure in austenitic and duplex stainless steel was a solution of fresh-made 50 vol.% HCl, 25 vol.% $HNO_3$ and 25 vol.% $H_2O$. Etching was performed for 10-25 seconds at room temperature. Precipitation hardening stainless steels were etched with Kalling's reagent no.1 (100 ml ethanol, 100 ml 32% HCl, 100 ml $H_2O$ and 4.5 g $CuCl_2$) for 3-4 seconds at room temperature. A Neophot 30 (Carl Zeiss) reflected light microscope equipped with a Photometrics CoolSnap CCD camera was applied for recording digital micrographs.

Micro-hardness indentations were performed on a Neophot 32 (Carl Zeiss) equipped with a Hanemann

*Table 3:*
*Procedure for metallographic preparation.*

| Grinding with SiC paper | | | |
|---|---|---|---|
| Grid | rpm | Force (max.) | Time [min.] |
| 120 | 125 | 150 N / 3 samples | To work-area |
| 220 | 125 | 150 N / 3 samples | 3 |
| 320 | 125 | 150 N / 3 samples | 3 |
| 500 | 125 | 150 N / 3 samples | 3 |
| 1000 | 125 | 150 N / 3 samples | 3 |
| 2400 | 125 | 150 N / 3 samples | 3 |
| 4000 | 125 | 150 N / 3 samples | 3 |

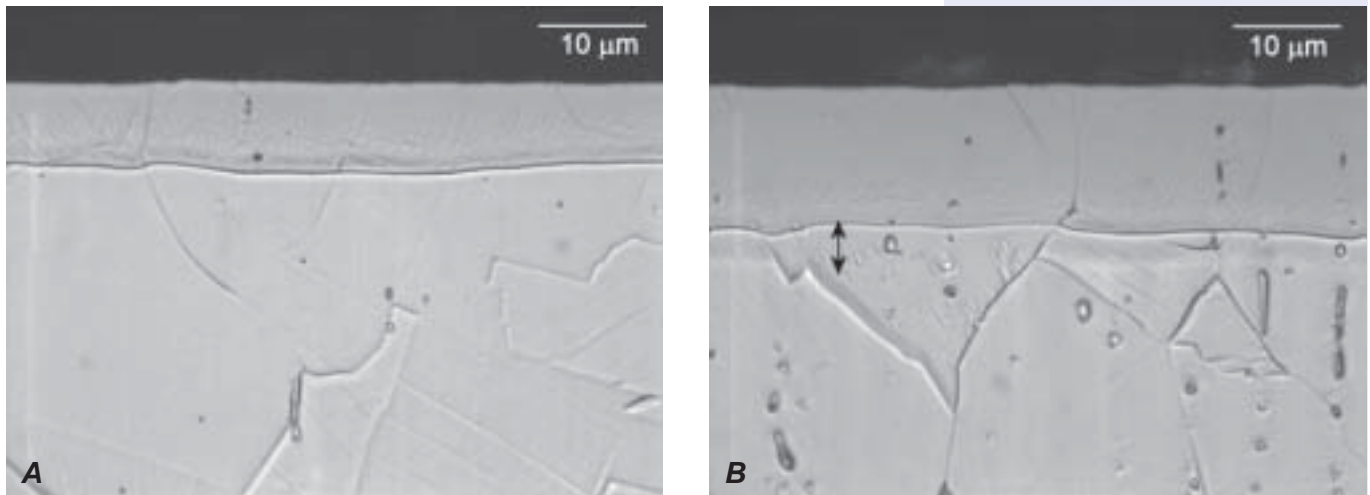| Polishing with polycrystalline diamonds | | | | | |
|---|---|---|---|---|---|
| Cloth | DP-Suspension P | Lubricant | rpm | Force (max.) | Time [min.] |
| DP-Mol | 3 µm | Green | 125 | 150 N / 3 samples | 3 |
| DP-Nap | 1 µm | Green | 125 | 150 N / 3 samples | 3 |

Fig.1: Micrographs of nitrided AISI 316 (nitrided at 718 K for 22 h). A) $K_N$ = 0.293 bar $^{-1/2}$ and B) $K_N$ = 2.49 bar $^{-1/2}$

micro-hardness tester from Carl Zeiss. A load of 6.25 g was used. Micrographs of the indentations were taken with polarised mono-chromatic light and an 100x planapochromatic oil immersion objective on the above-mentioned Neophot 30. The lengths of the diagonals of the indentations were measured from the digitally recorded micrographs.

A Bruker AXS D8 X-ray diffractometer, equipped with a Cr anode and a set of Göbel mirrors in the incident beam was used for identification of the crystallographic phases present in the samples and for determination of lattice strains (caused by residual stress).

## 3. Results and discussion

### 3.1. Austenitic stainless steel AISI 304 & AISI 316

#### 3.1.1. Nitriding

The austenitic stainless steels are the most commonly applied steel grades, especially grades AISI 304 and AISI 316. The major difference between AISI 304 and AISI 316 is the presence of the alloying element Mo in the latter; Mo provides enhanced corrosion resistance, particularly in chloride containing atmospheres. The resulting microstructures after gaseous nitriding of AISI 316 at 718 K at two different nitriding potentials - but otherwise identical conditions - are depicted in Fig.1. The surface adjacent region is transformed into $\gamma_N$ upon nitriding. The mirror-like finish of the untreated surfaces was maintained after nitriding. Evidently, the development of $\gamma_N$ depends strongly on the applied nitriding potential, in particular when considering the layer thickness. Presuming local equilibrium between nitrogen in the gas mixture and nitrogen in the solid state (at the sur-
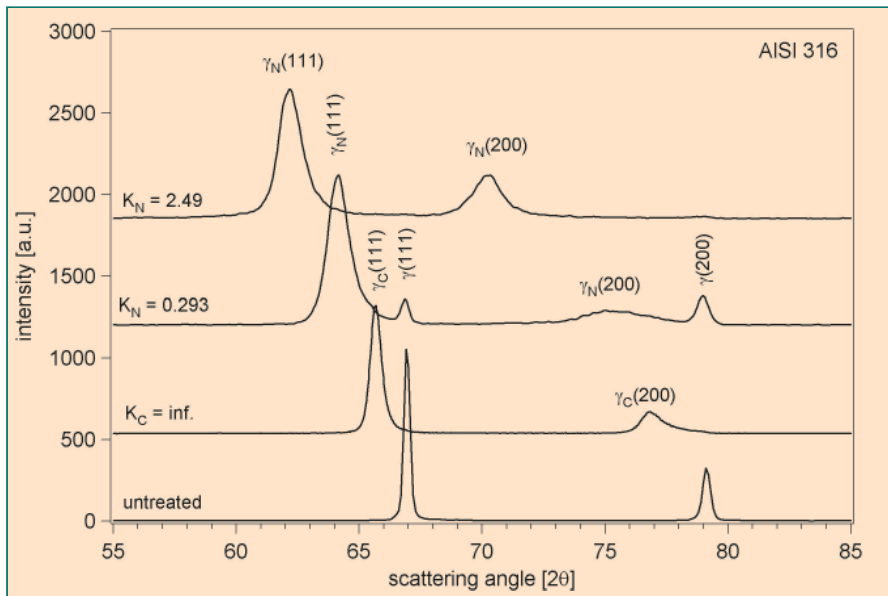
Fig. 2: X-ray diffractograms of nitrided and carburised AISI 316 measured with Cr $K_\alpha$ radiation. Nitriding: 22 h / 718 K with the nitriding potentials $K_N$ = 0.293 bar$^{-1/2}$ and $K_N$ = 2.49 bar$^{-1/2}$. Carburising: 6 h. / 780 K / $K_C$=∞.

face), applying a higher nitriding potential corresponds to a higher nitrogen content in the solid state [7]. Consequently, a higher driving force for inward diffusion of nitrogen is obtained. The $\gamma_N$ layers appear practically featureless, whereas the austenite substrate contains distinct microstructural features, viz. grain boundaries. This difference in appearance is caused by selective etching of the substrate, i.e. $\gamma_N$ has a higher electrochemical potential than the nitrogen-free austenitic substrate. What appears to be a phase boundary parallel to the surface is in fact a sharp interface caused by selective etching. The single-phase nature of the modified surface is observable in the microscope; grain boundaries are distinguishable in the expanded austenite near the substrate interface - waning slowly as the surface is approached and the nitrogen content increases (this is not observable in Fig. 1A). The microstructure in Fig.1B contains an interesting feature at the $\gamma_N$ / austenite interface (indicated): a clearly visible zone of a few microns is present, which is not an artefact caused by etching. The explanation could be found in the solubility product for trapping of nitrogen by chromium. A small amount of nitrogen may be dissolved into austenite before trapping of nitrogen by chromium occurs, i.e. before the solubility product is exceeded. Con-
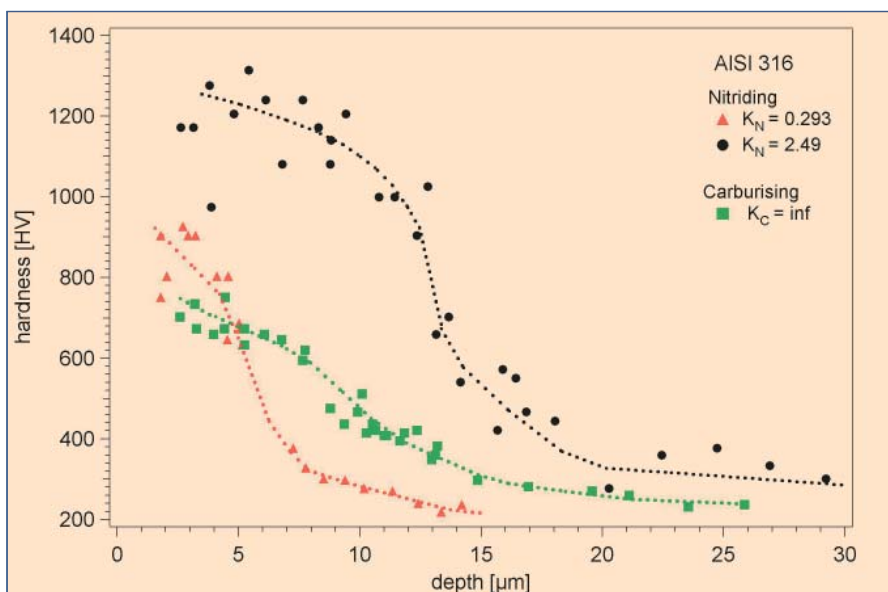


Fig. 3: Hardness-depth profiles of nitrided and carburised AISI 316. Nitriding: 22 h / 718 K with the nitriding potentials $K_N$ = 0.293 bar$^{-1/2}$ and $K_N$ = 2.49 bar$^{-1/2}$; the surface hardness as measured by indentation into the surface was 1417 HV and 1585 HV for $K_N$ = 0.293 bar$^{-1/2}$ and $K_N$ = 2.49 bar$^{-1/2}$, respectively. Carburising: 6h / 780 K / $K_C$=∞; the surface hardness as measured by indentation at the surface was 926 HV. Lines are drawn to guide the eye.
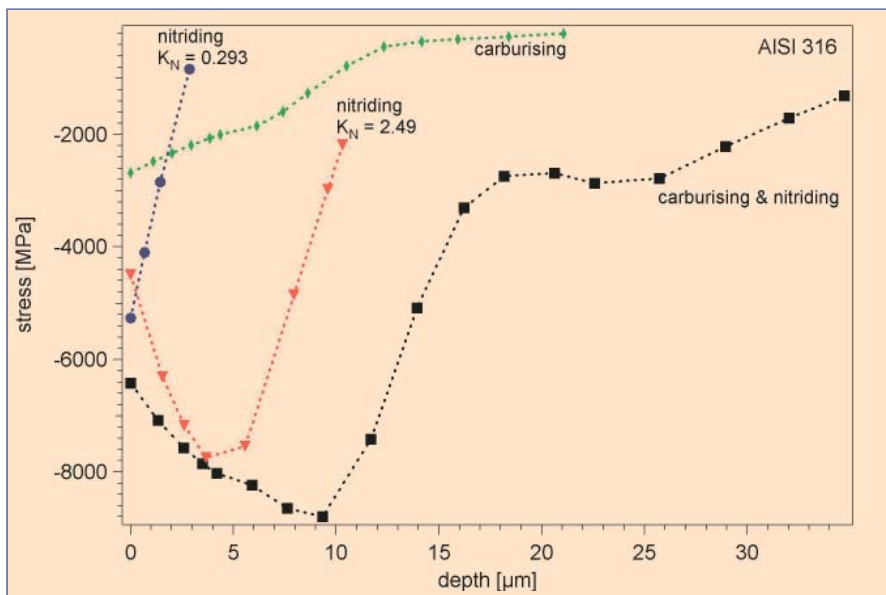
Fig. 4: Residual stress profiles for $\gamma_N$ and $\gamma_C$ layers in AISI 316 obtained by X-ray diffraction. Carburising: 793 K/ 2.5 h / 90% CO + 10% $H_2$. Nitriding: 22 h / 718 K with the nitriding potentials $K_N$ = 0.293 bar $^{-1/2}$ and $K_N$ = 2.49 bar $^{-1/2}$. Carburising and nitriding: 793 K / 2 h / 30% CO + 70% $H_2$ and 713 K / 23 h / $K_N$ = 1.14.

sequently, the zone observed is probably austenite with a low content of nitrogen. When the solubility product is exceeded, trapping occurs and a sudden increase in concentration takes place, this is the sharp "boundary" observed in the micrographs.

X-ray diffraction analysis showed that the nitrogen content is significantly higher in the sample nitrided at the highest nitriding potential (Fig.2). Comparing the diffractograms for the nitrided samples with the untreated material clearly shows that Bragg reflections (peaks) are shifted to lower 2θ angles. This is caused – primarily - by dissolution of nitrogen which causes a dilation of the f.c.c. lattice (hence the name expanded austenite), although residual stress and stacking faults also play a role in this respect. Consequently, the highest nitrogen content is in the sample nitrided at the highest nitriding potential. Peaks originating from the austenitic substrate are visible in the sample nitrided at $K_N$ = 0.293 bar$^{-1/2}$, thus stating that the thickness of the $\gamma_N$ layer is not as thick as for the sample nitrided at $K_N$ = 2.49 bar$^{-1/2}$. The broadening of the peaks for the nitrided samples is a consequence of the nitrogen concentration gradient in the analysed volume and an anticipated high density of microstructural defects in the $\gamma_N$ layer, i.e. stacking faults, dislocations etc.

The hardness-depth profiles presented in Fig. 3 show a large difference between the samples nitrided at different nitriding potentials in terms of maximum hardness and depth. However, the shapes of the profiles are similar: A smooth decrease near the surface followed by a sharp drop in hardness at a position close to the "layer/substrate" interface (Fig. 3). For a nitriding potential of $K_N$ = 2.49 bar$^{-1/2}$ the hardness falls from approximately 1000 HV to 500 HV within a few micrometres. The hardness values measured directly at the surface with the same load give 1585 HV and 1417 HV for $K_N$ = 2.49 bar$^{-1/2}$ and $K_N$ = 0.293 bar$^{-1/2}$, respectively. Evidently, a layer of expanded austenite is very hard and the transition from the hardened zone to the (soft) substrate occurs within a few microns, consistent with the micrographs in Fig.1. The systematically higher hardness value determined at the surface as compared to that close to the surface in a cross section, is explained from the enormous compressive residual
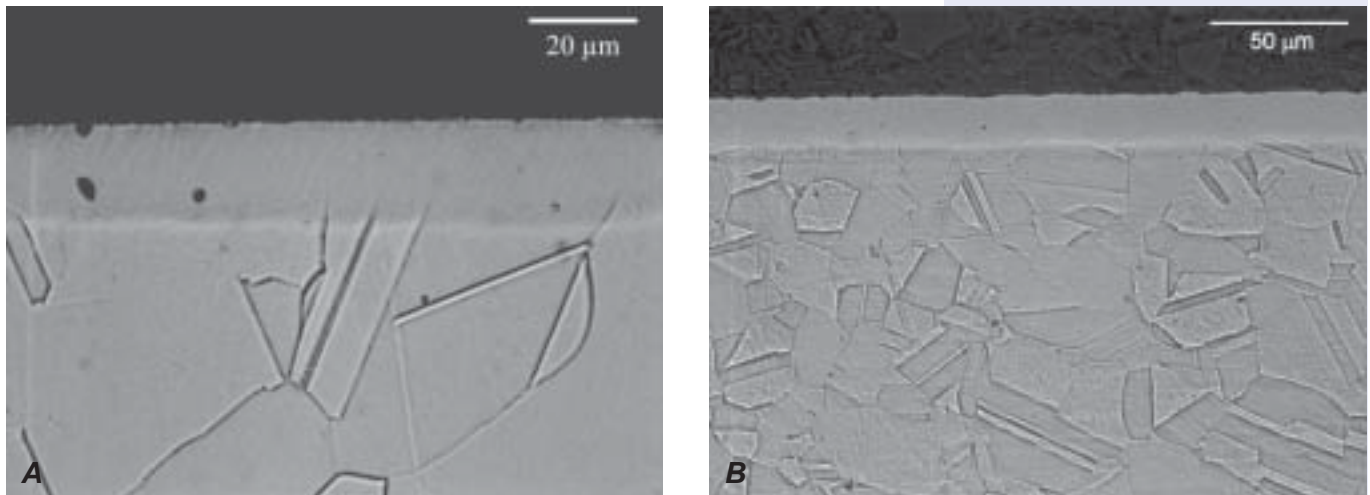
*Fig. 5. Micrographs of carburised stainless steel. A) AISI 316 / 780 K/ 6 h / $K_C$ = ∞). B) AISI 316L / 783 K/ 4 h / 40 vol.% CO + 60 vol.% $H_2$).*

stresses in the layer (see below). These high compressive residual stresses affect the indentation at the surface but have relaxed in the cross sections.

The residual stress depth profiles obtained by X-ray diffraction stress-analysis are given in Fig. 4. Huge compressive stresses are present in the $\gamma_N$ layers reaching even 8 GPa for a nitriding potential of $K_N$ = 2.49 bar$^{-1/2}$. Similar to the hardness depth profiles the stress depth profiles exhibit an abrupt drop when the substrate interface is approached. For the highest nitriding potential of $K_N$ = 2.49 bar$^{-1/2}$ the stress actually falls in the surface adjacent zone; the origin of this phenomenon can be attributed to, in particular, incipient crack formation. However, other stress relaxation mechanisms, such as production of stacking faults in $\gamma_N$ and possibly in the substrate, should also be taken into account. It is normally concurred upon that compressive stresses impose favourable fatigue properties in surface engineering of surfaces. In the present case unprecedented compressive stresses in the order of several GPa's are obtained, which may imply an improvement of the fatigue properties of thermochemically treated austenitic stainless steel.

### 3.1.2. Carburising of AISI 316

Cross sections of carburised AISI 316 and AISI 316L are presented in Fig. 5. It is evident that relatively thick layers of approximately 20 µm of carbon expanded austenite ($\gamma_C$) were obtained within a relatively short carburising time (e.g. 4 hours). The transition from the substrate to the transformed zone ($\gamma_C$) is not as pronounced as for nitriding, which is probably due to a lower interstitial atom content in $\gamma_C$ as compared to $\gamma_N$ and a smoother transition from the treated

case to the core. The grain boundaries from the substrate continue into $\gamma_C$ – fading out as the surface is approached (higher C contents) (Fig. 5A). $\gamma_C$ is not attacked by the applied etchant, as is especially evident in Fig. 5B. This, as for nitriding, hints at a higher electrochemical potential of $\gamma_C$ as compared to austenite.

The X-ray diffraction pattern of carburised AISI 316 is shown in Fig. 2. $\gamma_C$ is identified as the only phase present in the surface adjacent region, i.e. within the information depth for the probing X-ray beam. A marked difference is observed as compared to nitrided AISI 316; a smaller shift of the austenite peaks to lower $2\theta$, which indicates a substantially lower content of the interstitially dissolved atoms, provided that nitrogen and carbon induce a similar distortion in the f.c.c. lattice. The asymmetrical (200) austenite peak in Fig. 2 indicates a depth-gradient of the carbon content in the near surface zone. The distinct peaks for the carburised sample indicate a smooth concentration gradient and lower defect density in $\gamma_C$ layers as compared to $\gamma_N$ layers.

The hardness-depth profile of carburised AISI 316 is characterised by a relatively smooth transition from the surface to the substrate (Fig. 3). The hardness is considerably lower than for nitriding, but still significantly higher than the hardness of the substrate. Measured directly at the surface with the same load a value of 926 HV was obtained, which, as compared to a substrate hardness of 200-300 HV, is a significant increase.

The stress-depth profiles of carburised stainless steel have smooth transition from the surface to the substrate (Fig. 4) contrary to the stress depth profiles for nitrided samples. The maximum compressive stress is significantly lower also, which directly can be attributed to a significantly lower content of interstitial carbon as compared to nitrogen.

### 3.1.3. Nitrocarburising and combinations of carburising and nitriding

Micrographs of consecutively carburised and nitrided AISI 316 and nitrocarburised (cold worked) AISI 304 are depicted in Fig. 6. The combination treatment produces a relatively thick layer of expanded austenite of approximately 25-30 µm (Fig. 6A). The layer consists actually of two separate zones with a somewhat diffuse interface (which was clearly observed in the microscope, but is difficult to see in the present micrograph); the outer zone is $\gamma_N$ and the inner zone is $\gamma_C$. Conversely, the nitrocarburised sample shows a distinct separation of the $\gamma_N$ and $\gamma_C$ layers, with the $\gamma_C$ layer closest to the austenite substrate (as indicated in the micrograph in Fig. 6B).
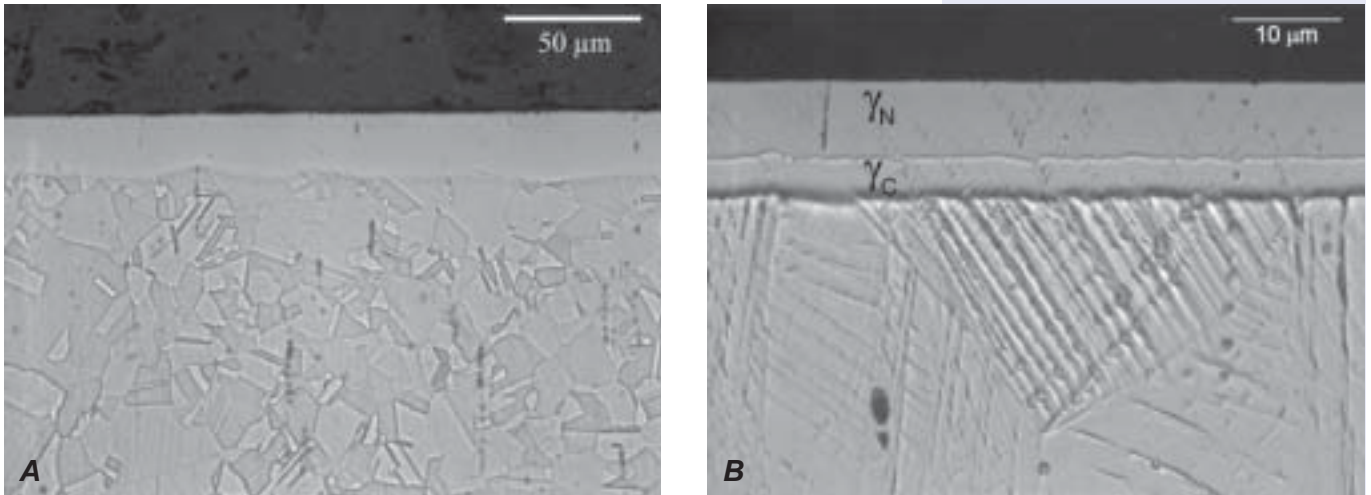
Fig. 6. Micrographs of A) carburised and subsequently nitrided AISI 316 and B) nitrocarburised AISI 304.
A) carburising: 773 K / 4 h / $K_C=\infty$), subsequent nitriding: 713 K / 18.5 h / $K_N = \infty$.
B) 693 K / 19 h / 10% Ar + 54% $NH_3$ + 22% $H_2$ + 14% $C_3H_6$.

The X-ray diffractogram of carburised and nitrided AISI 316 shows that two different types of expanded austenite are present (Fig. 7). The peaks of $\gamma_N$ are shifted more than $\gamma_C$ and are most dominant, because $\gamma_N$ has the highest interstitial atom content and is located closest to the surface. The expanded austenite peaks (without distinction between carbon and nitrogen expanded austenite) are broad, which is indicative of a very broad composition range.
The X-ray diffraction pattern does not indicate the development of carbides or nitrides during treatment.
The hardness depth profile depicted in Fig. 8 shows the combined effect of nitrogen and carbon expanded austenite. In the near sur-
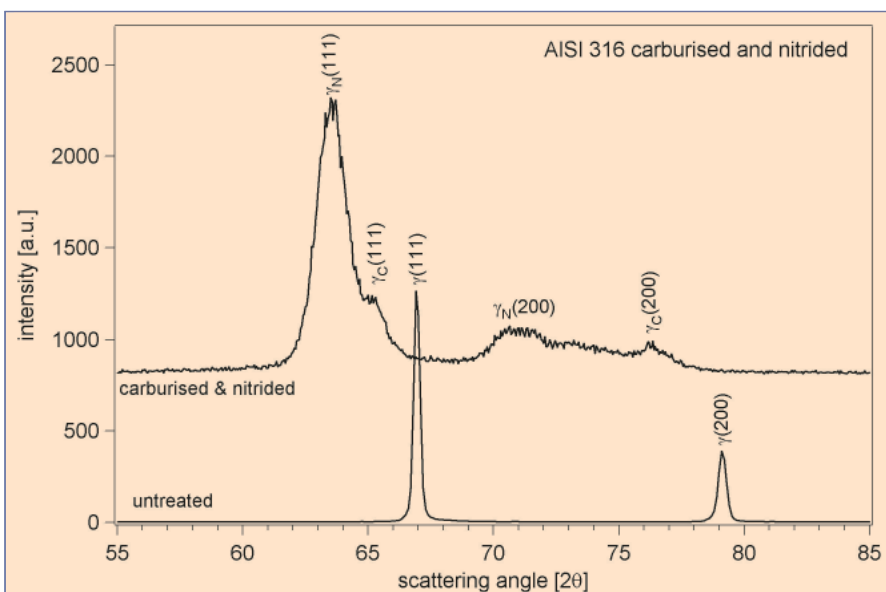


Fig. 7: X-ray diffraction pattern of AISI 316 carburised (773 K / 4 h / $K_C = \infty$) and subsequently nitrided (713 K / 18.5 h / $K_N = \infty$). Cr $K_\alpha$ radiation.
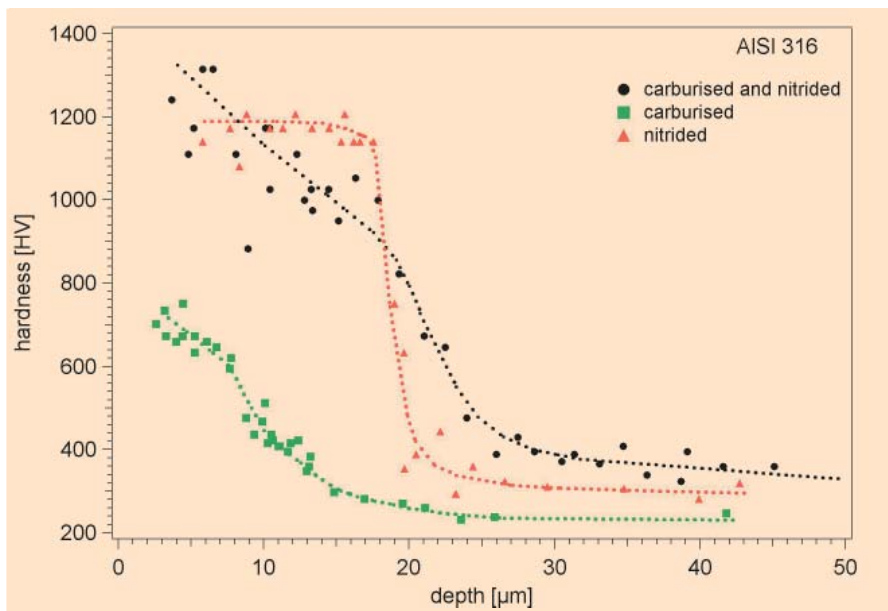
face region the hardness is approximately 1200 HV, the same as for nitriding only under similar conditions. The hardness decreases smoothly to a depth of approximately 18 μm followed by a steeper transition to the low substrate hardness. The profiles for nitriding and carburising are effectively added to give this characteristic profile. Hence, $\gamma_C$ has the role of a transition zone between the very hard $\gamma_N$ zone and the soft substrate. The drop in hardness from 1200 to 400 HV occurs over a much broader region for the combination treatment than for nitriding only (cf. Fig. 8).

The residual stress depth profile shows a similar picture: the stress profile is smoother as compared to nitriding only (Fig. 4). The $\gamma_C$ layer located between the $\gamma_N$ layer and the austenite substrate acts as a transition zone, i.e. smoothes the stress gradient inherent to $\gamma_N$ / austenite layers. On comparing the various profiles in Fig. 4 it is evident that the stress profile for the combination treatment can be patched from the individual profiles for nitriding and carburising. The technological aspects of a combination of $\gamma_N$ and $\gamma_C$ layers comprise an increased load-bearing capacity due to the underlying $\gamma_C$ layer (overall layer thickness is greatly improved), and a smooth case/core transition which is anticipated to provide more favourable fatigue properties and to prevent spalling of the hard $\gamma_N$ "layer".

It should be evident that a combination of nitrogen and carbon expanded austenite, either by a combination of nitriding and carburising or by nitrocarburising, allows depth profile tailoring of one or more material properties (e.g. hardness and residual stress). An important process parameter for such tailoring is the combination of carburising and nitriding potentials.

### 3.2. Duplex stainless steel

Nitriding of duplex stainless steel alloys is also possible as evidenced by the micrographs in Fig. 9. The basic microstructure of duplex stainless steel consists of austenite grains dispersed in a ferritic matrix. The austenite and ferrite regions have different compositions as a consequence of the partitioning of the ferrite- and austenite-forming alloying elements during heat treatment (cooling).
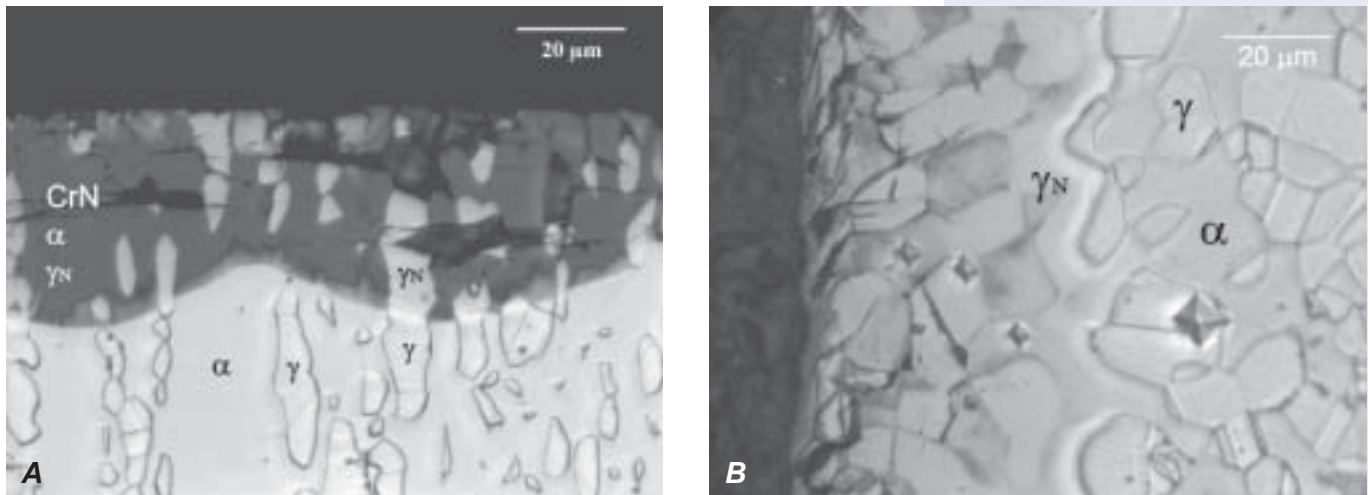
Fig. 9: Micrographs of nitrided duplex stainless steel. A) AISI 329 / 723 K / 23 h / $K_N$ = ∞. B) SAF 2507 / 708 K / 17 h / $K_N$ = ∞.

Nitriding of AISI 329 at 723 K produced a thick layer with marked differences between austenite and ferrite (Fig. 9A). The nitriding temperature of 723 K is clearly too high with regard to development of $\gamma_N$ in ferrite, but the increased temperature clearly demonstrates the differences between ferrite and austenite (nitriding below 698 K produces $\gamma_N$ in both austenite and ferrite).

The dark region in Fig. 9A is former α phase; the darkening is attributed to the presence of CrN precipitates smaller than the resolution of reflected light microscopy (= 0.15 μm for the present conditions). Evidently, these precipitates have developed prior to the α→γ transformation, because a shade of grey is also observed as a thin layer ahead of the α/γ interface (Fig. 9A), whilst such shading is absent for $\gamma_N$ on former γ. The development of CrN precipitates in α phase (and not in γ phase) is consistent with the higher Cr content in α, which induces a higher driving force for CrN development, and the possibility of coherent nucleation of CrN in α through a favourable crystallographic orientation relation between CrN and α (cf. Ref.18).

The superduplex SAF 2507 shows a different nitriding response than AISI 329 (Fig 9B). A thick layer of $\gamma_N$ has formed in both ferrite matrix and austenite grains. The austenite grains show clear signs of plastic deformation (slip), owing, in part, to the very large compressive stresses which develop in the $\gamma_N$ layer. The resulting microstructure clearly suggests that the applied nitriding potential and nitriding temperature were too high. Most likely, precipitates of CrN have formed in the surface adjacent region (the first formed $\gamma_N$), which was strongly mechanically affected prior to nitriding (cold-worked structure). The enormous increase in hardness (up to 1500 HV) is evident from the hardness indentation marks (Fig. 9B.).
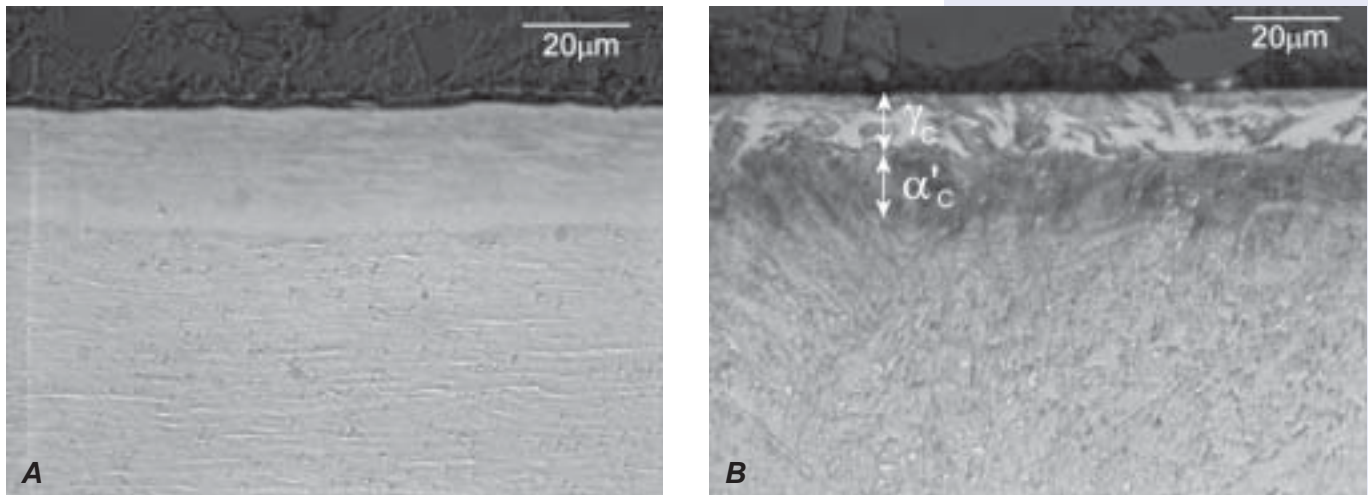
Fig.10: Micrographs of A) nitrided Nanoflex® (698 K / 16 h / $K_N$ = inf) and
B) carburised Corrax® (781 K / 19 h / $K_C$ = inf).

### 3.3. Precipitation hardening stainless steel

Precipitation hardening stainless steels are steels that are subjected to an annealing treatment in order to improve mechanical properties, viz. hardness. The topic of gaseous thermochemical treatment of precipitation hardening stainless steel is more thoroughly dealt with in reference [19]. The amount of bulk hardening depends on annealing time/temperature (and degree of deformation).
Interestingly, the temperature/time applied for low temperature surface hardening coincides with the temperature/time for maximum bulk hardness [19]. This enables simultaneous bulk hardening and surface hardening, i.e. a single step process.

The microstructures of nitrided Sandvik Nanoflex® and carburised Uddeholm Corrax® are depicted in Fig.10. Nitriding of Nanoflex® gives a layer thickness of more than 20 µm. The surface layer actually consists of two phases, nitrogen expanded austenite, $\gamma_N$, and nitrogen expanded martensite $\alpha'_N$ [19]. The applied nitriding potential determines the phases formed; a high nitriding potential favours the formation of $\gamma_N$ whilst a low nitriding potential favours the formation of $\alpha'_N$. The formation of $\alpha'_N$ is likely to occur prior to the formation of $\gamma_N$. Dissolving nitrogen into (cubic) martensite causes a tetragonal expansion leading to nitrogen expanded martensite. At some threshold nitrogen content the $\alpha'_N$ transforms into $\gamma_N$, due to the strong austenite stabilizing effect of nitrogen. This nitrogen threshold value is only reached for high nitriding potentials. A similar transformation mechanism is prevailing during carburising, which is clearly observed for carburising of Corrax® (Fig.10B). The separation of carbon expanded austenite, $\gamma_C$, and carbon expanded martensite, $\alpha'_C$, is clearly visible (also indicated in Fig.10B).

The surface hardness of nitrided or carburised precipitation harden-
ing stainless steels is generally significantly higher than for auste-
nitic stainless steels; hardness values in excess of 2000 HV are not
uncommon. Hardness depth profiles for Nanoflex® and Corrax®
are shown in Fig.11. Nitriding of Nanoflex® yields a surface hard-
ness of more than 2000 HV to a depth of approximately 20 µm, fol-
lowed by a relatively sharp drop in hardness. The bulk hardness has
increased from an as-delivered hardness of 400 HV to 684 HV. This
increase in bulk hardness is caused by the simultaneously occurring
precipitation hardening of the bulk during the nitriding treatment.
The hardness depth profile for carburised Corrax® shows a similar
surface hardness as for Nanoflex®, i.e. 2200 HV in the near surface
region. However, for Corrax® it is clearly observed that both carbon
expanded austenite and carbon expanded martensite are present;
a distinct drop in hardness is observed at the interface between $\gamma_C$
and $\alpha'_C$ (as indicated in Fig.11). The hardness depth profile is slow-
ly waning, yielding hardness values in excess of 1000 HV to a depth
of 30 µm. The bulk hardness of the material increases from the as-
delivered hardness of 330 HV to 540 HV as a result of carburising.
The transition from a very high surface hardness to the bulk hard-
ness appears over an extended region of several micrometers (anal-
ogously to the combination of $\gamma_C$ and $\gamma_N$ in austenitic stainless steel).
Hence, by adjusting the nitriding/carburising potential the hardness
depth profile can be tailored, by controlling the amounts of expanded
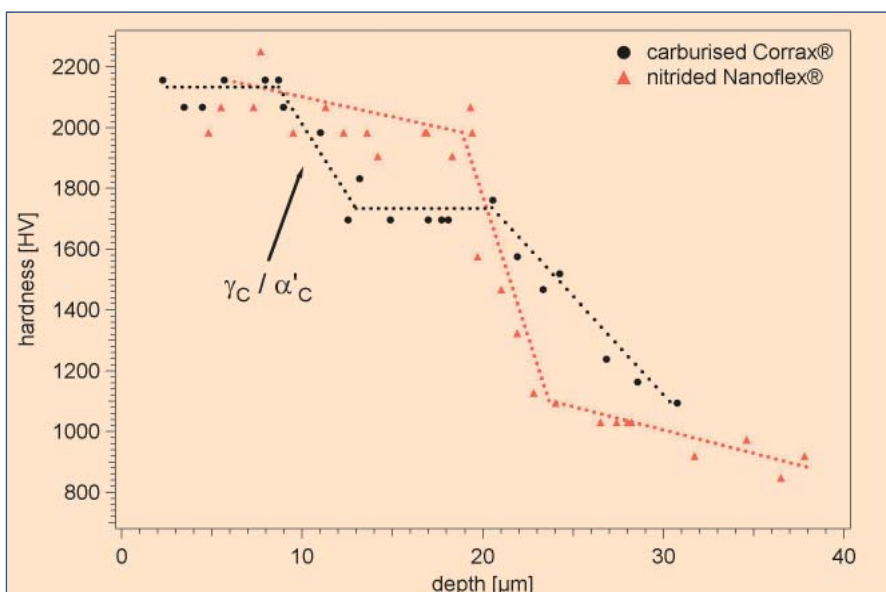austenite and expanded martensite.



Fig.11: Hardness-depth profiles of carbu-
rised Corrax® (781 K / 19 h / $K_C$ = inf) and
nitrided Nanoflex® (698 K / 16 h / $K_N$ = inf).
Lines are drawn to guide the eye.

### 3.4. Thermal stability of expanded austenite

The thermal stability of expanded austenite is an important issue as surface treated stainless steel parts may be exposed thermally. Decomposition of expanded austenite, which is a thermally activated process, involves precipitation of chromium nitrides- or carbides. As a consequence, chromium is retracted from solid solution and the favourable corrosion properties of the stainless steel (expanded austenite) are lost. Another aspect of the thermal stability of expanded austenite relates to the nitriding/carburising process; if the temperature is too high or if the process time is too long chromium nitrides/carbides precipitate during the process. Fig.12 shows an example of nitriding AISI 316 at too high a nitriding temperature - CrN precipitates have developed along grain boundaries and more homogeneously adjacent to the surface.

In order to characterize the decomposition kinetics of nitrogen expanded austenite, homogenous stress-free synthesized $\gamma_N$ was produced by through-nitriding of micrometer-sized stainless steel thin foil. AISI 304L and AISI 316L $\gamma_N$ with controlled nitrogen contents were subjected to thermal analysis in a thermal analyzer capable of simultaneous differential thermal analysis and thermogravimetric analysis (the interested reader is referred to [8] where this topic is dealt with thoroughly). On basis of experimental non-isothermal results the isothermal stability of nitrogen expanded austenite was calculated (Fig.13).
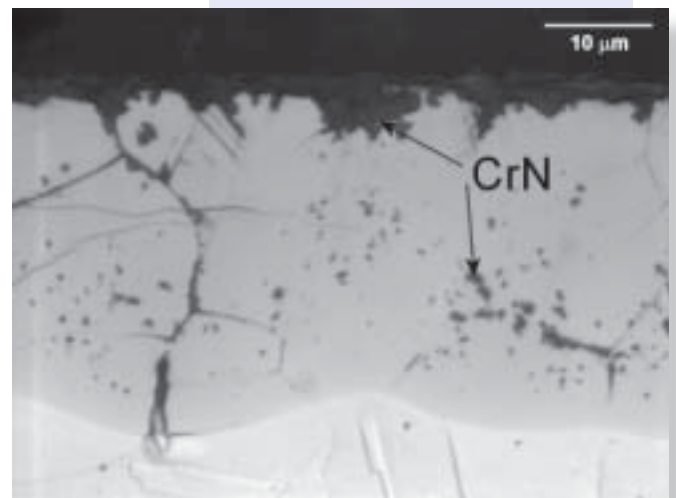


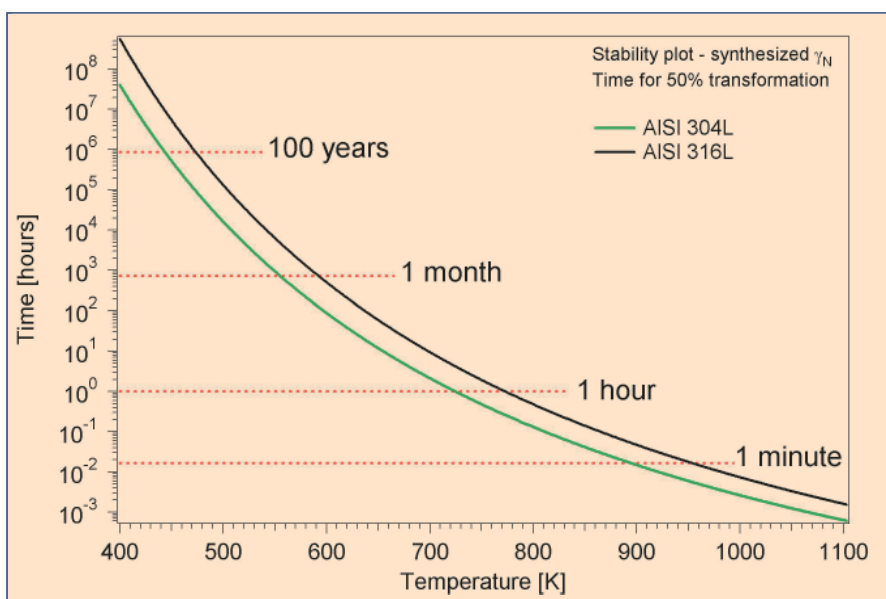Fig. 12. Micrograph of nitrided AISI 316 (T=753 K / 21 h / $K_N$ = inf).



Fig.13: Stability plot (temperature/time) of $\gamma_N$ in AISI 304L and AISI 316L.

Clearly, the presence of Mo in AISI 316L in comparison to AISI 304L has a significant effect on the thermal stability of $\gamma_N$ as the decomposition temperature is shifted to higher temperatures. The stability plot for AISI 316L states that it takes $\gamma_N$ 100 years to decompose if exposed to a temperature of 473 K (200°C), however for temperatures above, say, 800 K (527°C) it is a matter of minutes before decomposition occurs. It is also obvious from Fig.13 that the process parameters temperature and time for nitriding are a compromise between fast development of a $\gamma_N$ zone and slow development of CrN precipitates during treatment (Note in this respect that the foils used for the calculation of Fig.13 were nitrided 22 hours and cooled to room temperature before they were investigated with thermal analysis).
In AISI 304L $\gamma_N$ decomposed into CrN and ferrite ($\alpha$) after annealing, whereas AISI 316L $\gamma_N$ decomposed into CrN and austenite ($\gamma$). This difference can be related to the thermodynamic stability range of austenite in these materials and the temperature at which decomposition commences [8].

## 4. Conclusions

Low temperature gaseous thermochemical treatment of stainless steels gives rise to a transformation of the surface adjacent region into nitrogen and/or carbon expanded austenite. Expanded austenite layers are hard and exhibit excellent tribological and electrochemical properties. Nitrogen expanded austenite can be formed in several stainless steel grades, i.e. austenitic, duplex and precipitation hardening stainless steel. Technologically, the depth profiles of the material properties can be tailored; particularly, the combination of carburising and nitriding or nitrocarburising appears promising. Precipitation hardening stainless steel is a special case as surface hardening and bulk hardening occur simultaneously. The surface hardness in these steels may exceed 2000 HV and tailoring of depth profiles is possible by controlling the amount of expanded austenite and expanded martensite. Expanded austenite is not a stable "phase" and will decompose when thermally annealed for extended periods of time. The presence of the alloying element Mo in stainless steel improves the thermal stability of expanded austenite.

**References**
[1] K. Ichii, K. Fujimura and T. Takase: Technology Reports of Kansai University, 1986, 27, 135-144.
[2] S. Thaiwatthana, X. Y. Li, H. Dong and T. Bell: Surface Engineering, 2002, 18(6), 433-437.
[3] T. Christiansen and M.A. J. Somers: Scripta Materialia, 2004, 50, 35-37.
[4] Y. Sun, X. Li and T. Bell: Materials Science and Technology, 1999, 15, 1171-1178.
[5] Y. Sun, T. Bell, Z. Kolosvary and J. Flis: Heat Treatment of Metals, 1999, 1, 9-16.
[6] C. Blawert, H. Kalvelage, B. L. Mordike, G. A. Collins, K. T. Short, Y. Jirásková and O. Schneeweiss: Surface and Coatings Technology, 2001, 136, 181-187.
[7] T. Christiansen and M.A.J. Somers: Controlled dissolution of colossal quantities of nitrogen in stainless steel, Metallurgical Transactions A, in press.
[8] T. Christiansen and M.A.J. Somers: Decomposition kinetics of expanded austenite with high nitrogen contents, Zeitschrift für Metallkunde, in press.
[9] X. Y. Li, Y. Sun and T. Bell: Z. Metallkd., 1999, 90(11), 901-907.
[10] Y. Jirásková, C. Blawert and O. Scheeweiss: Phys. Stat. Sol. (a), 1999, 175, 537-548.
[11] E. Menthe and K.-T. Rie: Surface and Coatings Technology, 1999, 116-119, 199-204.
[12] X. Y. Li: Surface Engineering, 2001, 17(2), 147-152.
[13] Y. Sun and T. Bell: Wear, 1998, 218, 34-42.
[14] S. Mändl, R. Günzel, E. Richter and W. Möller: Surface and Coatings Technology, 1998, 100-101, 372-376.
[15] X. Tian and P. Chu: Scripta Materialia, 2000, 43, 417-422.
[16] B. Normand, A. Pierre and J. Pagetti: Corrosion Science, 1995, 37(10), 1537-1549.
[17] M.A. J. Somers, T. Christiansen and P. Møller: Case hardening of stainless steel, Danish Patent DK174707 B1 and PCT/DK03/00497
[18] M.A. J. Somers, R. M. Lankreijer and E. J. Mittemeijer: Philosophical Magazine A, 1989, 59(2), 353-378.
[19] R. B. Frandsen, T. Christiansen, M.A. J. Somers; Surface and Coatings Technology, in press, available online 4 june 2005.